ICSV14
Cairns • Australia
9-12 July, 2007

14th International Congress on Sound & Vibration

LARGE EDDY SIMULATION OF JET NOISE

X Wu[1], G J Page[1], J K Luff[1], J J McGuirk[1] and W A McMullan[1]

[1]Dept. of Aero. and Auto. Engineering, Loughborough University
Loughborough, Leicestershire LE11 3TU, U.K.
j.j.mcguirk@lboro.ac.uk

Abstract

Methods for the accurate prediction of far-field jet noise emitted by aeroengines have been under development for some time. To achieve this, one essential requirement is capture of the turbulence dominated noise sources in the jet shear layers and, for the low frequency contribution to noise, simulation of the dynamically active large eddies at the end of the jet potential core and just downstream. The method described in the present paper follows a hybrid approach, whereby an LES technique is first used to predict the unsteady characteristics of the turbulent noise sources in jet shear flows. This is then coupled to an integral method for acoustic propagation (Kirchhoff method). The nozzle geometry is included in the calculation domain and a fine mesh (~15 million cells) is used to improve resolution of the initial jet shear layer. The method is applied to a high Reynolds number (Re = 10^6) cold turbulent round jet issuing into stagnant surroundings. Experimental data for mean and turbulent velocity components are used to assess the accuracy of the LES predictions. The directivity pattern of the predicted far-field noise is used to assess the performance of the hybrid method and to indicate the benefit, particularly for sideline noise, of inclusion of the nozzle in the calculation.

1. INTRODUCTION

The noise signature of a civil turbofan aeroengine is made up of fan noise, turbomachinery noise, and jet noise. Some of these sources are tonal in nature, whilst others, e.g. jet noise, are broadband and more difficult to model accurately. Engine manufacturers have made substantial efforts to understand the various sources and identify techniques to assist designers meet the stringent noise regulations. For high bypass ratio engines, jet noise is the most prominent source at full power take-off conditions. This has lead to nozzle designs being sought that can effect jet noise reduction. One example is the use of trailing edge 'serrations', which have shown substantial noise reduction in both model scale and flight tests [1], although it is far from clear as to the physical mechanism by which this is achieved. Methods for accurate prediction of jet noise have been under development for some time. Compressible DNS studies have begun to appear [2], which capture, directly and simultaneously, flowfield and acoustic characteristics, including both source and far-field regions. These studies are very useful in improving our understanding of the fundamentals of noise generation. But, DNS is computationally expensive, and currently limited to jet Reynolds numbers far below those typical of applications, and nozzle geometries far simpler than current designs. Hence, applicable noise prediction methods are based either on empirically-obtained databases, or on the coupling of steady RANS CFD (incorporating a two-equation turbulence model) and an acoustic propagation method (typically Lighthill acoustic analogy or a Linearised Euler (LEE) method), e.g. [3]. However, whilst this approach has had reasonable success at predicting the noise of simple round jets, the turbulence models in RANS procedures were calibrated for 2D shear layers/self-similar flows. Their ability to deliver accurate turbulence information in 3D flowfields such as in the near-field of serrations is doubtful [4]. An alternative hybrid approach has received significant attention in recent years [5], [6]. This is the use of an LES technique coupled to an integral method for acoustic propagation (Kirchhoff surface method) [7]. The LES captures the unsteady characteristics of the turbulent noise sources in jet shear flows, particularly the dynamically energetic large eddies at the end of the jet potential core. As long as the jet nozzle is included in the calculation and a fine enough mesh is used, the large scale structures responsible for noise levels at the peak directivity angles can be resolved sufficiently to reproduce good agreement with experimental data [8]. For high Re this leads to demanding mesh resolution requirements, implying grids of O(10) million points for the jet shear region. This argues that optimum efficiency is achieved via a hybrid route where LES is restricted to the noise source region, and the unsteady pressure field on its periphery is extracted from the simulation and drives a propagation model to produce far-field acoustics.

The present paper describes results from such a hybrid approach being developed for jet noise prediction [8]. The methodology is assessed against recent experimental data [9]. The following outlines the computational methodology and provides some numerical details. A comparison of LES and RANS solutions with experimental data for flowfield and turbulence statistics is given. Finally, the far-field acoustic signature is compared with measurements.

2. MATHEMATICAL FORMULATION

2.1 Governing Equations

The integral form of the spatially- and Favre-filtered compressible Navier-Stokes equations is expressed in vector form for a stationary volume Γ enclosed by a surface $\partial\Gamma$ as:

$$\frac{\partial}{\partial t}\iiint_{\Gamma} \mathbf{Q}\,\mathrm{d}V + \iint_{\partial\Gamma} \mathbf{F}(\mathbf{Q})\cdot\mathbf{n}\,\mathrm{d}S - \iint_{\partial\Gamma} \mathbf{G}(\mathbf{Q})\cdot\mathbf{n}\,\mathrm{d}S = 0 \tag{1}$$

where $\mathbf{n}$ is the outward pointing unit vector orthogonal to $\partial\Gamma$ and t is time. $\mathbf{Q}$ is the state vector, $\mathbf{F}$ is the convective flux vector and $\mathbf{G}$ is a vector containing viscous, conductive and sub-grid scale stress/heat flux terms; in Cartesian tensor notation, these may be written:

$$\mathbf{Q} = \left[\bar{\rho}, \bar{\rho}\tilde{u}_i, \bar{\rho}\tilde{E}\right] \qquad \mathbf{F}(\mathbf{Q}) = \left[\bar{\rho}\tilde{u}_j, \bar{\rho}\tilde{u}_i\tilde{u}_j + \bar{p}\delta_{ij}, \bar{\rho}\tilde{H}\tilde{u}_j\right]$$
$$\mathbf{G}(\mathbf{Q}) = \left[0, \bar{\sigma}_{ij} + \tau_{ij}^{SGS}, \bar{q}_j + \bar{q}_j^{SGS} + \tilde{u}_i(\bar{\sigma}_{ij} + \tau_{ij}^{SGS})\right] \tag{2}$$

The usual ideal gas law and caloric equation of state connect the filtered static pressure to the state vector. The spatial filtering used to derive this LES form of the governing equations results in additional terms which must be modelled using a Sub-Grid Scale (SGS) model.

$$\tau_{ij}^{SGS} = 2\mu_{SGS}(\tilde{S}_{ij} - \frac{1}{3}\tilde{S}_{mm}\delta_{ij}) - \frac{2}{3}\bar{\rho}k_{SGS}\delta_{ij} \quad \tilde{S}_{ij} = \frac{1}{2}(\frac{\partial \tilde{u}_i}{\partial x_j} + \frac{\partial \tilde{u}_j}{\partial x_i}) \quad q_j^{SGS} = \frac{Cp\mu_{SGS}}{\sigma_{SGS}}\frac{\partial \tilde{T}}{\partial x_j} \tag{3}$$

In this work the standard Smagorinsky model [10] with Van Driest near-wall damping [11] was used to specify the sub-grid scale viscosity in terms of the magnitude of the filtered strain rate tensor and a filter width related to the cube root of the local cell volume. In addition, Werner-Wengle wall functions [12] were applied in near wall regions.

$$\mu_{SGS} = \bar{\rho}(C_S\Delta)^2\bar{S} \qquad \bar{S}=(2\tilde{S}_{ij}\tilde{S}_{ij})^{\frac{1}{2}} \qquad \Delta = (\Delta x\Delta y\Delta z)^{\frac{1}{3}} \tag{4}$$

All calculations presented here have used the Smagorinsky model constant (C_s) set to 0.15.

3. NUMERICAL TECHNIQUES

3.1 LES Formulation

Multi-block, structured, curvilinear, body-fitted grids allow accurate resolution of reasonably complex geometry, with only a moderate overhead in computational time compared to single block Cartesian grids. Mature grid generation technology allows high quality grids to be generated with control over skewness and expansion, which can have an adverse affect on LES solution quality. Hence, this approach has been used here as the basis of a finite volume cell-centred discretisation of the governing equations. The base methodology was originally developed for RANS solutions (using a k-ε model) and applied to both high speed compressible flows with shock waves, and low speed incompressible problems [13], [14]. The LES capability was developed for the prediction of multiple impinging jets [15]. Spatial fluxes are computed by combination of cell-centred values on each side of a cell face. For example, the convective flux **F(Q)** (excluding the pressure term) can be simplified to:

$$\iint_{\partial\Gamma} \mathbf{F}(\mathbf{Q}) \cdot \mathbf{n}\, dS = \iint_{\partial\Gamma} \mathbf{Q}(\mathbf{u} \cdot \mathbf{n})\, dS \tag{5}$$

The normal component of velocity **u.n** at the cell face is computed by central differencing. The value of the state vector **Q** is found using a MUSCL scheme; for example, for **u.n** > **0** :

$$\mathbf{Q}_l = \mathbf{Q}_{L-1} + \frac{1}{4}\left[(1-\kappa)\tilde{\Delta}_- + (1+\kappa)\tilde{\Delta}_+\right]\mathbf{Q}_{L-1} \tag{6}$$

l denotes a face with cell $L-1$ on the left and cell L on the right. The backward and forward difference limited operators are defined via:

$$\tilde{\Delta}_- = \text{minmod}(\Delta_-, \beta\Delta_+) \qquad \tilde{\Delta}_+ = \text{minmod}(\Delta_+, \beta\Delta_-) \tag{7}$$

$$\Delta_-(\mathbf{Q}_L) = \mathbf{Q}_L - \mathbf{Q}_{L-1} \qquad \Delta_+(\mathbf{Q}_L) = \mathbf{Q}_{L+1} - \mathbf{Q}_L \tag{8}$$

$$\text{minmod}(x, y) = \text{sgn}(x)\max\left\{0, \min\left[|x|, y\,\text{sgn}(x)\right]\right\} \tag{9}$$

The controlling parameter κ defines the discretisation scheme: κ = -1 is a second order upwind scheme, κ = 1/3 is a third order scheme, κ = 1/2 is a low truncation error second order upwind scheme, and $\kappa = 1$ is a central difference scheme. The latter is used with the limiter disabled, and with an additional smoothing term to suppress the odd-even decoupling (Rhie and Chow [16]). The mass, momentum and energy equations are solved sequentially with a spatially implicit scheme. The mass equation is transformed into a pressure-correction equation to allow the computation of low speed flows without any preconditioning. Temporal advancement is via a low storage Runge-Kutta third order scheme. The code has been parallelised to allow use of PC clusters; the multi-block structure allows straightforward domain decomposition-based parallelisation and calculations can be carried out on both shared memory machines (using OpenMP) and distributed memory machines (using MPI).

3.2 Noise Propagation to the Far-field

The far-field acoustic solution is evaluated from a linear Kirchhoff formulation [7] applied on a control surface surrounding the nonlinear field. The sound pressure at observer locations is obtained in terms of a surface integral of fluctuating pressure and its normal and time derivatives on the control surface. Further details of the Kirchhoff surface integration method can be found in [7] and [17]. The pressure perturbation at location x at time t is evaluated as:

$$p'(\mathbf{x},t) = \frac{1}{4\pi}\int_S \left[\frac{p'}{r^2}\frac{\partial r}{\partial n} - \frac{1}{r}\frac{\partial p'}{\partial n} + \frac{1}{c\,r}\frac{\partial r}{\partial n}\frac{\partial p'}{\partial t} \right]_{\tau_r} dS \qquad (10)$$

τ_r denotes evaluation at retarded time, related to observer time by $\tau_r = t - r/c$, where r is the distance between a point on the control surface and the observer and c is the speed of sound in the far-field region. The surface S should enclose all sound generating structures and be placed in a region where the flow is governed by a linear wave equation and no vorticity crosses the surface. It is common practice to use a surface open at its ends. It has been shown [5], [17] that errors so introduced are small, hence this practice has been adopted here.

4. RESULTS

4.1 Test Case, Geometry and Grid Generation.

A suitable test case for the present purposes is a single round jet in stagnant ambient at high Re (O(10^6)), with mean/turbulent flowfield data as well as far-field sound data. Until recently, such an ideal case was not available. Early mean flow and acoustics data were obtained by Stromberg et al [18] for an M=0.9 jet, but at very low Re=3600; turbulence statistics were provided at Re=95,500 by Hussein et al [19], but at low M=0.165. Fortunately, the experiments of Power et al [9] and Jordan et al [20] offer detailed flowfield and acoustic surveys for a high subsonic jet at Re ~10^6 and have been selected here. Cold jet data at M=0.75 are used here, with a jet nozzle exit diameter and velocity of 50mm and 255m/s. As in [8], the nozzle geometry was included in the calculation. Uzun and Hussaini [21] have shown that careful mesh design is needed if initial jet shear layer development is to be accurately resolved. Their work used ~50 million nodes at Re = 10^5 with a near wall spacing of y_+ ~ 1 for the cells at nozzle exit. The predictions here are based on our earlier work [8], which indicated that a wall-function treatment (near wall spacing y_+ ~30) and a fine mesh in the circumferential direction should be sufficient to capture the initial shear layer development without too high mesh numbers. Unlike the work of Andersson et al [6], for the same test case (but at a reduced Re = $5\text{x}10^4$), the predictions below were carried out at Re ~10^6. Fig. 1 shows the 3-block topology and grid design used.

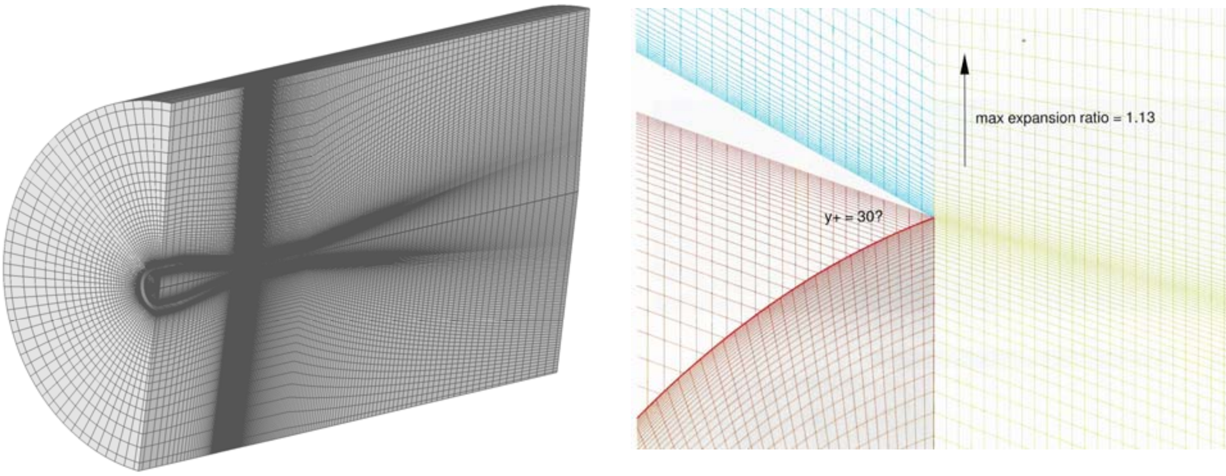

Fig. 1 Solution domain, mesh topology and close up of nozzle exit mesh

The inlet plane was set $5D_j$ upstream of nozzle exit; the radial extent of the domain was $10D_j$ and the jet development was captured for $30D_j$ downstream. The finest grid consisted of 420 nodes axially (120 inside the nozzle), 100 radially (40 inside the nozzle) and 360 circumferentially (~15 million cells in total). The mesh was non-uniform, axial spacing being smallest at nozzle exit and radial spacing finest in the jet shear layer. A RANS calculation was used to estimate the spread of the shear layer so the fine mesh region was angled to follow this. Grid expansion factors were smaller than 1.1.

4.2 Mean velocity and turbulence statistics.

Initial predictions were carried out using a RANS k-ε approach for later comparison. Fig. 2 shows the predicted turbulence kinetic energy. The high energy in the shear layer regions is clearly identified, and the unsteady dynamics of these turbulent fluctuations are inherently connected to the noise source. Of course the unsteadiness of the large energy containing eddies is not predicted by the RANS approach, whereas it emerges naturally from the LES as

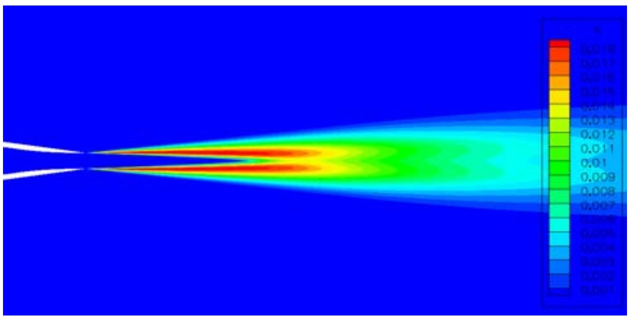

Fig.2 Turbulence energy - RANS predictions

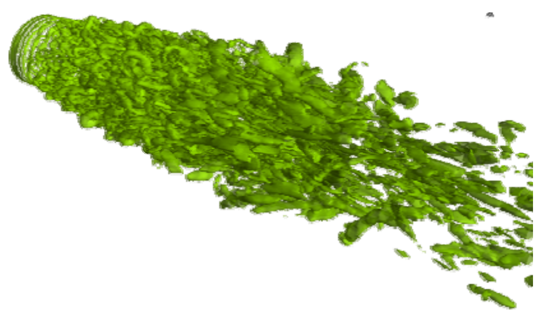

Fig. 3 Eddy structure visualisation - LES

shown in Fig. 3. This indicates that the nozzle inclusion, boundary layer resolution and high density mesh has not completely resolved the initial shear layer, which still shows some evidence of vortex ring structures, but these breakdown into fully turbulent behaviour very quickly, unlike in many LES predictions (even at much lower Re) where the SGS model has to be altered before this happens. The importance of including the nozzle in the prediction is shown in Fig. 4 via a mean Mach No. profile at $x/D_j=1$ compared to the data of Stromberg [18]. The improvement in this early stage of shear layer development is clear to see, enabled partly by the nozzle inclusion, and partly by the fine circumferential grid resolution, as shown

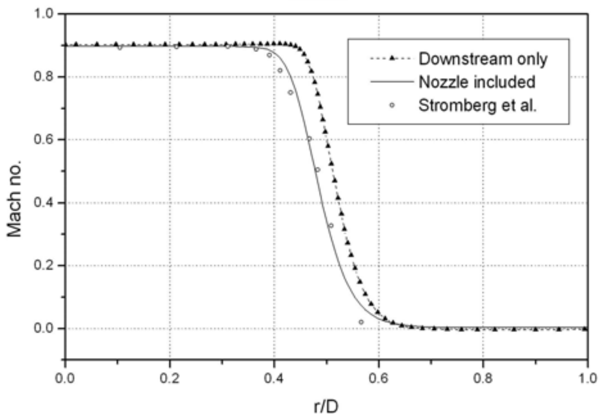

Fig. 4 LES predicted shear layer profile

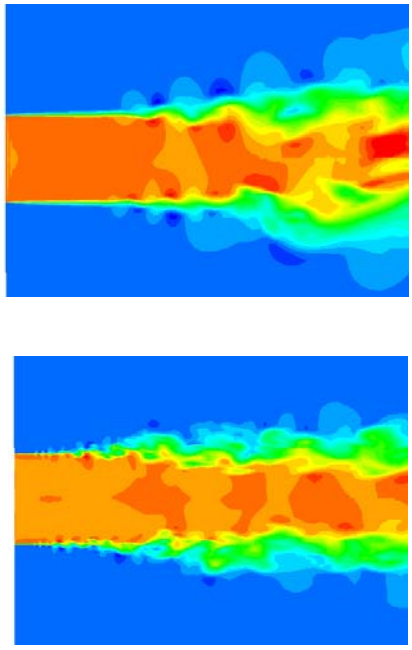

Fig. 5 LES predicted Mach Contours

in Fig. 5; this compares coarse azimuthal resolution (103 cells, top) against a finer azimuthal mesh (360 cells, bottom). The lower picture clearly shows the capture of smaller structures and an earlier breakdown into fully turbulent flow. When the initial shear layer is laminar (top picture), the breakdown happens later, but is much more energetic, creating very large scale structures, and usually leading to an underprediction of the potential core length. Comparison with the mean velocity measurements of [9] is shown in Fig. 6 for both RANS (k-ε) and LES predictions. The potential core length is still slightly underpredicted by the LES method. Using U/U_{jet}=0.95 to define the potential core end, the current prediction is L_{PC} = 5.85, as opposed to 5.45 in the LES reported in [6] and 6.5 in the measurements [9]. L_{PC} is significantly overpredicted by the RANS method (8.5). As a consequence, the two radial profiles shown at x/D_j=1 and 5 are in general better predicted by the LES method. The steep gradient at x/D_j=1 is better resolved and although the LES profile is slightly too wide at x/D_j=5 (consistent with a shorter potential core), the RANS profile shows an appreciable flat region in the central zone as the end of the potential core is still far from being reached.

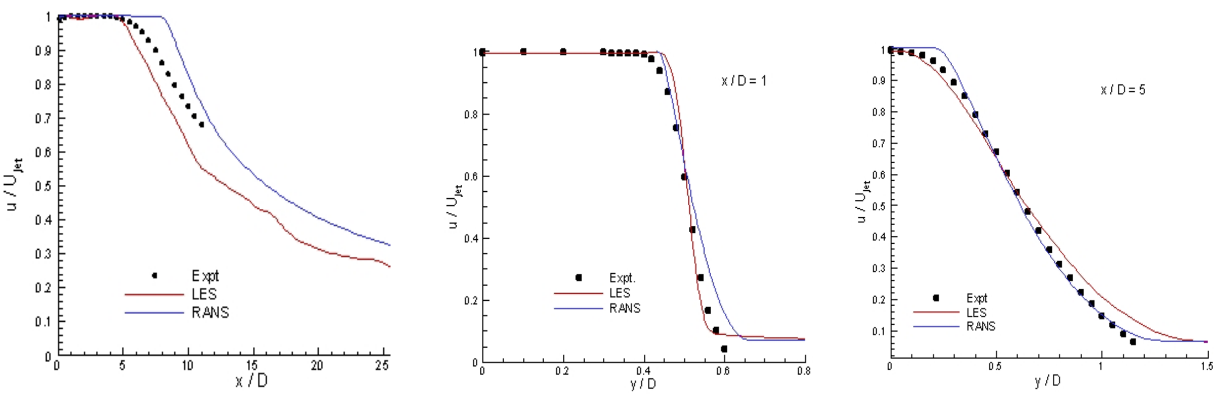

Fig. 6 Mean axial velocity, RANS and LES predictions against Expt. Data [9]

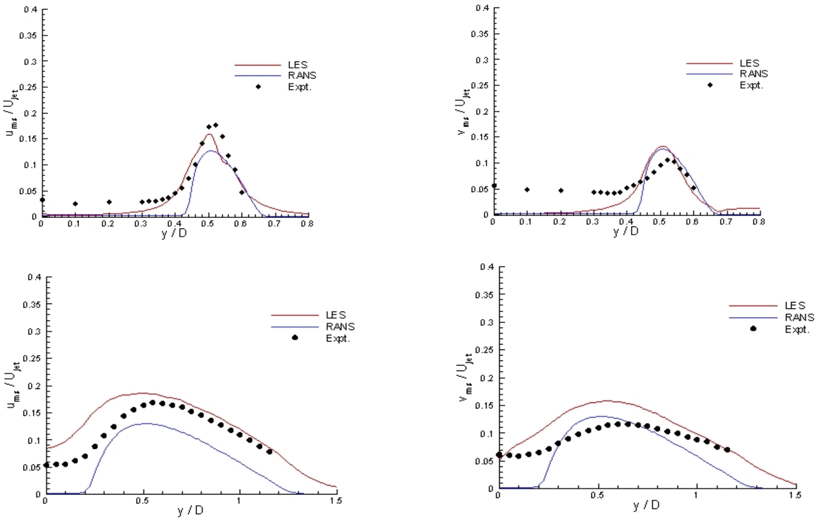

Fig. 7 Turbulence intensities (left axial, right radial); profiles at x/D_j=1 (top), x/D_j=5 (bottom) RANS and LES predictions against Expt. Data [9]

The accuracy of predicting turbulent fluctuations is assessed in Fig. 7. This presents axial and radial turbulence intensities at two stations, x/D_j=1 and x/D_j=5. Once again the benefit of the LES approach compared to the RANS method in capture of turbulence statistics is underlined. The anisotropy (axial intensity greater than radial) and the shape of the profiles are much improved in the LES predictions.

4.4 Far-field acoustics.

To evaluate the acoustic far-field generated by the turbulent sources captured in the LES prediction, a conical open-ended Kirchhoff surface (3.5R_j height at nozzle exit and 9R_j downstream) was used to predict the acoustic pressure pattern in a rectangular plane stretching to the far-field. An instantaneous pressure field produced is illustrated in Fig. 8; clearly a strong radiator of sound is located at the end of the potential core

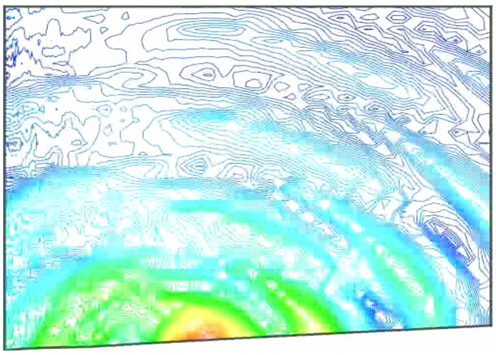

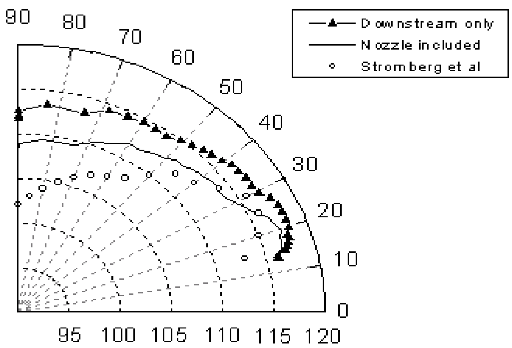

Fig. 8 Instantaneous acoustic field   Fig. 9 OASPL prediction with/without nozzle

The sound pressure level was computed for observers located on an arc 30D_j away from the nozzle centre (Fig. 9) compared with the data of Stromberg [18]. The directivity pattern is very similar to the measurements, with peak directivity at ~30^0. Note the improvement in the sideline prediction at 90^0 with inclusion of the nozzle, caused by the improved turbulence physics capture of the high frequency noise sources in the initial shear layer.

5. SUMMARY AND CONCLUSIONS

The paper has reported on work to develop a hybrid technique for the prediction of jet noise. The turbulent mean and fluctuations were simulated using an LES method. The resulting unsteady pressure around the jet is propagated to the far-field using a surface integral method. A finite-volume, multi-block structured approach was adopted. A mesh of 15 million cells was used to simulate a round jet at Re = 10^6. Comparison of mean and turbulent velocity statistics and far-field sound directivity pattern with data is encouraging.

6. ACKNOWLEDGEMENTS

Funding for this work was provided by UK EPSRC Grant GR/S43207/01.

REFERENCES

[1] E. Nesbitt, T. R. Elkoby, T. R. S. Bhat, P. J. R. Strange, C. Mead, “Correlating model scale and full-scale test results of dual flow nozzle jets”, AIAA-2002-2487, *8th AIAA/CEAS Aeroacoustics Conference*, Breckenridge, CO, USA, June 2002.

[2] J. B. Freund, “Noise sources in a low Reynolds number turbulent jet at Mach 0.9”, *Journal of Fluid Mechanics,* **438**, 277-305, (2001).

[3] C. K. W. Tam, L. Auriault, “Jet mixing noise from fine-scale turbulence”, *AIAA Jnl.*, **37**, 145-153, (1999).

[4] G. J. Page, J. J. McGuirk, M. Hossain, R. H. Self, A. Bassetti, “A CFD coupled acoustics approach for coaxial jet noise”, AIAA-2003-3286, *9th AIAA/CEAS Aeroacoustics Conf.*, Hilton Head, SC, USA, 2003.

[5] M. L. Shur, P. R. Spalart, M. Kh. Strelets, A. K. Travin, “Towards the prediction of noise from jet engines”, *Int. Journal of Heat and Fluid Flow*, **24**, 551-561, (2003).

[6] N. Andersson, L-E. Eriksson, L. Davidson, "A study of Mach 0.75 Jets and their radiated sound using LES", AIAA-2004-3024, *10th AIAA/CEAS Aeroacoustics Conference,* Manchester, UK, June 2004.

[7] A. Lyrintzis, “A review: the use of Kirchhoff’s method in computational Aeroacoustics”, *ASME Journal of Fluids Engineering*, **116**, 665-676, (1994).

[8] X. Wu, I. H. Tristanto, G. J. Page, J. J. McGuirk, “Influence of nozzle modelling in LES of turbulent free jets”, AIAA-2003-2883, *11th AIAA/CEAS Aeroacoustics Conference,* Monterey, CA, USA, May 2005.

[9] O. Power, F. Kerherve, J. Fitzpatrick, P. Jordan, “Measurements of turbulence statistics in high subsonic jets”, AIAA-2004-3021, *10th AIAA/CEAS Aeroacoustics Conference,* Manchester, UK, June 2004.

[10] J. Smagorinsky, "General circulation experiments with the primitive equations, I: The basic experiment", *Monthly Weather Review*, **91**, 99-164, (1963).

[11] E. R. Van Driest, "On turbulent flow near a wall", *Journal of Aeronautical Science*, **23**, 1007-1011, (1956).

[12] H. Werner and H. Wengle, “Large Eddy Simulations of turbulent flow over and around a cube in a plane channel”, *Proceedings of Turbulent Shear Flows 8*, 155-168, Springer Verlag, Berlin, Germany, 1991.

[13] G. J. Page, H. Zhao, J. J. McGuirk, “A parallel multi-block Reynolds Averaged Navier Stokes method for propulsion installation applications”, *Proc. of 12th Int. Symp. Air-Breathing Eng.*, 864-876, Australia, 1991.

[14] H. Salman, D. Jiang, G. J. Page, J. J. McGuirk, "Linear and non-linear turbulence model predictions of vortical flows in lobed mixers", *The Aeronautical Journal*, **108**, 65-73, (2004).

[15] G. J. Page, Q. Li, J. J. McGuirk, “LES of impinging jet flows relevant to vertical landing aircraft”, AIAA-2005-5226, *23rd AIAA Applied Aero. Conf.*, Toronto, Canada, June 2005.

[16] C. M. Rhie and W. L. Chow, "Numerical study of the turbulent flow past an aerofoil with trailing edge separation", *AIAA Journal*, **21**, 1525-1535, (1983).

[17] J.B. Freund, S. K. Lele, P. Moin, “Calculation of the radiated sound field using an open Kirchhoff surface”, *AIAA Journal*, **34**, 909-916, (1996).

[18] J. L. Stromberg, D. K. McLaughlin, and T. R. Troutt, "Flowfield and acoustic properties of a Mach Number 0.9 jet at a low Reynolds number", *Int. Jnl. of Sound and Vibration*, **72**, 159-176, (1980).

[19] H. J. Hussein, S. P. Capp, W. K. George, "Velocity measurements in a high Re momentum conserving axisymmetric turbulent jet", *Journal of Fluid Mechanics,* **258**, 31-75, (1994).

[20] P. Jordan, Y. Gervais, "Modelling self- and shear noise mechanisms in anisotropic turbulence", AIAA-2003-8743, *9th AIAA/CEAS Aeroacoustics Conf.*, Hilton Head, SC, USA, 2003.

[21] A. Uzun and M.Y. Hussaini, "High frequency noise generation in the near nozzle region of a jet", AIAA 2006-2499, *12th AIAA/CEAS Aeroacoustics Conference,* Cambridge, MA, USA, May 2006.